Electronic Journal «Technical Acoustics»
http://www.ejta.org

2006, 8

Z. C. Zheng*, B. K. Tan, W. Li

Department of Mechanical and Nuclear Engineering, Kansas State University, Manhattan, Kansas 66506, USA

On compact Green's functions and asymptotic expansions for flow-induced sound predictions

Received 16.03.2006, published 21.04.2006

Both compact Green's functions and asymptotic expansions are widely used to analytically predict sound generated by low Mach number ($M << 1$) fluid-dynamic sources, where the acoustic compactness of the source region is satisfied. By mathematically investigating the detailed assumptions involved in each of the two methods and by using two classical examples of flow noise problems, it is shown that the applicability of compact Green's function is restricted to a receiver location, *r*, at the acoustic far-field with $\omega r / c_o \to \infty$ where ω is the frequency and c_o is the speed of sound, and that the solution from matched asymptotic expansions can be applied less restrictively starting at $\omega r / c_o \sim 1$. Significant differences between the two solutions are shown when $\omega r / c_o \sim 1$. In the acoustic far-field, the solutions from the two methods are analytically proved identical.

1. INTRODUCTION

After Lighthill [1, 2], sound generated by fluid flow can be directly related to the near-field fluid dynamic parameters. Using Lighthill's analogy, two approaches can be developed to analytically predict low-Mach-number-flow sound: compact Green's functions (CGF) and matched asymptotic expansions (MAE). Examples of using these two methods include (but are not limited to) vortex related far-field sound (e.g., [3–7]). Both of the methods take advantage of the low-Mach-number condition and the acoustic compactness of the source to facilitate the mathematical analysis. However, there can be confusion regarding to the applicability and limits of these two methods. Particularly, in many cases the consistency of the results from these two methods is not readily obvious, a situation that deems a careful investigation. It is relatively clear that in using MAE, the spatial dimensions in the acoustic region are reduced with a factor of Mach number (*M*) to match the near-field expansions, but it is not the case that the CGF is truncated to the same order of Mach number. The goal of this paper is to investigate mathematically the detailed assumptions involved in each of the two methods and to sort out the compatibility and, at the same time, the differences between them. Two classical examples, flow over an oscillating cylinder and a vortex outside a cylinder, are used to demonstrate the comparison procedures. Sample results are calculated for explanation of the analytical solutions.

*Corresponding author, e-mail: zzheng@ksu.edu

2. COMPARISON OF ASSUMPTIONS EMPLOYED IN THE TWO METHODS

In both of the methods, the flow is low Mach number, $M << 1$, where $M = U_o / c_o$, U_o is the characteristic velocity of the near-field, and c_o is the speed of sound. Since both of the methods are used for acoustic calculation, the far-field condition must be satisfied, which is $r >> l$ where r is the distance of the receiver location from the source, and l is the characteristic length of the source. The acoustic compactness of the source is also required in both MAE and CGF. That is,

$$\omega l / c_o \sim O(M) << 1, \tag{1}$$

where ω is the frequency and O means "the order of".

In the MAE method, to match the near-field flow with the acoustic field, the spatial dimensions in the acoustic field is usually reduced in the order of M, i.e., $X_i = Mx_i$, where x_i is the receiver location in the acoustic field, and X_i is the rescaled outer spatial dimensions to match the inner flow solution. The time scale in the near-field is in the same order as that in the acoustic field (e.g., [6, 7]). It is then clear that in the MAE method, all the approximations are in $O(M)$. The receiver distance in the acoustic field is $O(l/M)$ away from the source,

$$r \sim l / M . \tag{2}$$

In addition, because the expansions only apply to low Mach-number flow, it implies the compactness of the source, Eq. (1). This condition restricts the characteristic size of the near-field source region to guarantee that the considered acoustic wave length is at least of $O(l/M)$. Notice this restriction is on the size of the source, rather than on the receiver location in the acoustic field. The restriction of the acoustic receiver location is imposed in Eq. (2), to be $O(l/M)$, which is in the same order as the acoustic wave length. In combining Eqs. (2) and (1), it can be deduced that

$$\omega r / c_o \sim O(1) . \tag{3}$$

In the CGF method, a mathematical requirement of the receiver location, $r \to \infty$, has to be satisfied (e.g., [3–5]). However, it has not been explicitly indicated at what order this requirement needs to be satisfied in terms of Mach number. A careful examination of the mathematical arguments employed to derive the CGF shows that this requirement imposes an extra restriction on the receiver location:

$$\omega \frac{r}{c_o} >> 1 . \tag{4}$$

This means that the receiver is located at the acoustic far-field. That is, the receiver distance has to be much larger than the considered acoustic wavelength. Evidently, the compact source condition, Eq. (1), and the low Mach-number assumption themselves do not guarantee that Eq. (4) can be satisfied at the same time. In order to satisfy both of the compactness and the far-field requirement (Eq. 4), the following condition has to apply:

$$\frac{r}{l} >> \frac{1}{M}. \tag{5}$$

By comparing the above equation with Eq. (3), it can be seen that, while only $l/r \sim O(M)$ needs to be satisfied in the MAE method, a more restrictive condition of $l/r \sim O(M^n)$ has to be satisfied where *n* is at least greater than unity.

While both Eq. (2) and Eq. (5) require that the receiver location is far away from the source when $M << 1$, the applicability regarding to the receiver location is more restrictive in CGF ($l/r \sim O(M^n)$) than that in MAE($l/r \sim O(M)$). At the acoustic far-field, the solutions from the two methods should be identical since both of them describe the same acoustic signal from the same source at the acoustic far-field. In some cases, these two solutions have the same expression. An example is the acoustic pressure produced by a vortex near a half-plane. In this case, the results from CGF (by Howe in Section 6.2.2. of [5]) and from MAE (by Crighton in [7]) are exactly the same. However, in two classical examples, i.e., an oscillating cylinder and a vortex outside a cylinder, the two solutions have different expressions and the consistency between the two solutions is not easily shown. They are discussed in the following two sections to further illustrate the difference in the applicable limit and consistency in the acoustic far-field in the two solutions.

3. SOUND GENERATED BY AN OSCILLATING CIRCULAR CYLINDER

The analytical solution for this problem was given by Dowling and Ffowcs Williams [8] which was developed based on conservation of momentum for inviscid flow. For a circular cylinder with radius of *a* oscillating at $x_1 = \varepsilon e^{i\omega t}$ and $x_2 = 0$, as shown in Fig. 1, the expression for the pressure fluctuation is

$$p(\vec{x},t) = \frac{\rho_o \omega \varepsilon c_o \cos\theta}{H_0^{(2)"}(\omega a/c_o)} H_0^{(2)'}(\omega r/c_o) e^{i\omega t}, \tag{6}$$

where $r = \sqrt{x_1^{\,2} + x_2^{\,2}}$ is the distance from the origin, and $H_0^{(2)}$ is the Hankel function of the second kind of order zero. Notice that this solution can be applied to both the near-field and the far-field, under the assumption that the flow is inviscid and low Mach number.

Kao [6] used the MAE method for this problem and derived the acoustic pressure fluctuation. The details of the procedure are in [6], and the result is rewritten here in a dimensional form:

$$p(\vec{x},t) = i\frac{\pi \rho_o \varepsilon \omega^3 a^2}{2c_o} \cos\theta H_1^{(2)}(\omega r/c_o) e^{i\omega t}, \tag{7}$$

where $H_1^{(2)}$ is the Hankel function of the second kind of order one.

It is expected that Eq. (6) reduce to Eq. (7). With the relations in [9], the Hankel function derivatives in Eq. (6) can be rewritten as

$$H_0^{(2)'}(z) = -H_1^{(2)}(z), \tag{8}$$

and

$$H_0^{(2)''}(z) = H_2^{(2)}(z) - \frac{1}{z} H_1^{(2)}(z). \tag{9}$$

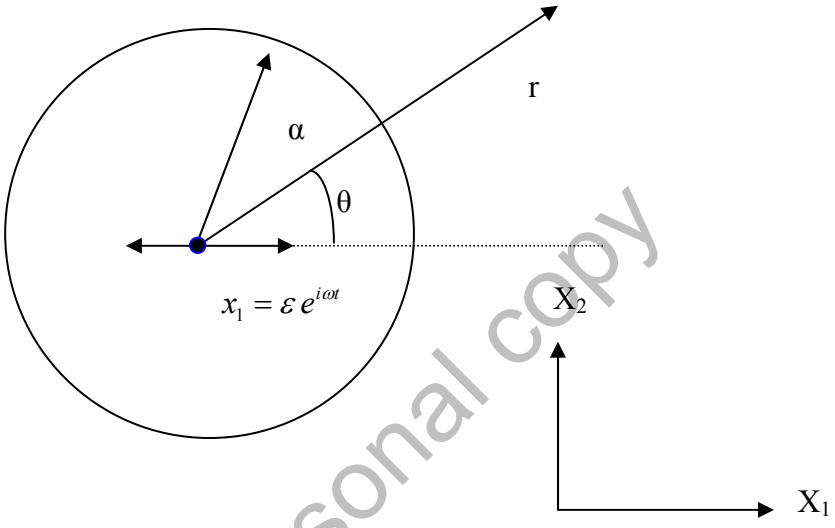

Figure 1. An oscillating cylinder

Under the condition of a compact source $\omega a / c_o << 1$, the asymptotic expressions of Hankel functions at small arguments give

$$H_0^{(2)''}(\omega a / c_o) \to \frac{2i}{\pi}\left(\frac{c_o}{\omega a}\right)^2. \tag{10}$$

Substitution of the Hankel function expressions of Eqs. (8) and (10) into Eq. (6) yields Eq. (7).

Since the details of using CGF for this problem is not shown in the literature, we present the derivation here following Howe [5]. The CGF for this two-dimensional problem can be expressed as (Eq. (6.1.5) in [5])

$$G(\vec{x}, \vec{y}, t-\tau) = \frac{\vec{x} \cdot \vec{Y}}{2\pi\sqrt{2c_o}\, r^{3/2}} \frac{\partial}{\partial t}\left\{\frac{H(t-\tau-r/c_o)}{\sqrt{t-\tau-r/c_o}}\right\}, \tag{11}$$

where H is the Heaviside step function, and $\vec{Y}(\vec{y})$ is the Kirchhoff vectors for the circular cylinder. The vector components, $\vec{Y}_j(\vec{y})$, represent the velocity potentials of incompressible

flow past the cylinder having unit speed in the *j* direction at large distance from the body. For flow over a circular cylinder, they can be expressed as

$$Y_j = y_j(1+\frac{a^2}{|\vec{y}|^2}), \tag{12}$$

where *j*=1, 2. For the fluctuating cylinder in this problem, the far-field fluctuation velocity potential can be expressed as

$$\phi(\vec{x},t) = -\int_{-\infty}^{\infty}\oint_S \upsilon_n(\vec{y},\tau)G(\vec{x},\vec{y},t-\tau)dS(\vec{y})d\tau, \tag{13}$$

where $\upsilon_n(\vec{y},\tau)$ is the surface normal velocity that can be expressed as

$$\upsilon_n(\vec{y},\tau) = n_i(\vec{y})U_i(\tau), \tag{14}$$

and $U_i(\tau)$ is the surface translational oscillation velocity, which is ($i\omega\varepsilon e^{i\omega\tau}$, 0) in this case. Notice since the contour integral in Eq. (13) is on the surface of the cylinder, the Kirchhoff vector in Eq. (12) can be expressed as

$$\vec{Y} = 2a(\cos\alpha,\sin\alpha), \tag{15}$$

and

$$n_i(\vec{y})U_i(\tau) = n_1U_1(\tau) = U_1(\tau)\cos\alpha, \tag{16}$$

where $U_1(\tau) = i\omega\varepsilon e^{i\omega\tau}$. Then substitute Eqs. (11) and (14) into Eq. (13), with expressions in Eqs. (15) and (16), to get

$$\phi(\vec{x},t) = -\frac{a^2}{\pi\sqrt{2c_o}r^{3/2}}\frac{\partial}{\partial t}\int_{-\infty}^{t-r/c_o}\frac{U_1(\tau)}{\sqrt{t-\tau-r/c_o}}d\tau\int_0^{2\pi}x_1\cos^2\alpha + x_2\sin\alpha\cos\alpha)d\alpha. \tag{17}$$

Therefore, the far-field pressure fluctuation is

$$p(\vec{x},t) = -\rho_o\frac{\partial\phi}{\partial t} = \frac{\rho_o a^2}{\sqrt{2c_o r}}\cos\theta\frac{\partial^2}{\partial t^2}\int_{-\infty}^{t-r/c_o}\frac{U_1(\tau)}{\sqrt{t-\tau-r/c_o}}d\tau. \tag{18}$$

To use Eq. (18), U_1 is taken real and equal to

$$U_1(\tau) = -\omega\varepsilon\sin(\omega\tau) = \omega\varepsilon\cos\left(\frac{3\pi}{2}-\omega\tau\right). \tag{19}$$

A formula in [5] (on p. 142) is used to express the integration in Eq. (18). Noticing the expression in [5] is for $\omega < 0$ and here we assume $\omega > 0$, we have

$$\int_{-\infty}^{t-r/c_o}\frac{\cos(\beta-\omega\tau)}{\sqrt{t-\tau-r/c_o}}d\tau = \sqrt{\frac{\pi}{\omega}}\cos\left[\beta-\omega\left(t-\frac{r}{c_o}\right)+\frac{\pi}{4}\right], \tag{20}$$

giving the integration in Eq. (18) to be

$$\int_{-\infty}^{t-r/c_o} \frac{U_1(\tau)}{\sqrt{t-\tau-r/c_o}} d\tau = \int_{-\infty}^{t-r/c_o} \frac{\omega\varepsilon\cos(3\pi/2-\omega\tau)}{\sqrt{t-\tau-r/c_o}} d\tau$$
$$= -\varepsilon\sqrt{\pi\omega}\cos\left[\omega\left(t-\frac{r}{c_o}\right)-\frac{3\pi}{4}\right]. \tag{21}$$

By substituting the above integration into Eq. (18), the pressure becomes

$$p(\vec{x},t) = \left(\frac{\pi}{2}\right)^{1/2} \frac{\rho_o a^2 \varepsilon\omega^{5/2}}{\sqrt{c_o r}} \cos\theta\cos\left[\omega(t-r/c_o)-\frac{3\pi}{4}\right]. \tag{22}$$

Equation (22) is the acoustic pressure using the CGF method. According to the argument following Eq. (5), we would like to see how it compares with Eq. (7) under the acoustic far-field condition, Eq. (4). In fact, when $\omega r/c_o \to \infty$ the Hankel function in Eq. (7) can be expressed as [9]

$$H_1^{(2)}(\omega r/c_o) \to \sqrt{\frac{2c_o}{\pi\omega r}} e^{-i(\omega r/c_o - 3\pi/4)}. \tag{23}$$

Substitution of Eq. (23) into Eq. (7) with taking the real part leads to exactly Eq. (22).

Figure 2 contains sample plots of the acoustic pressure versus time using the MAE and CGF methods. The results are calculated using the MAE method, Eq. (7), and the CGF method, Eq. (22). Note that Eq. (7) is applicable for any values of $\omega r/c_o \sim O(1)$, while Eq. (22) is only valid in the acoustic far-field when $\omega r/c_o \to \infty$. In Fig. 2, the acoustic pressure is normalized with the coefficient in Eq. (22), $\sqrt{\pi}\rho_o a^2 \varepsilon\omega^{5/2}/\sqrt{2c_o r}$. With this normalization, the CGF solution behaves just as a sinusoidal function of time, while the MAE solution should asymptote to a sinusoidal function as in Eq. (22) when $\omega r/c_o \to \infty$. The time variation is in the range of ωt from 0 to 2π. A representative direction of the receiver location at $\theta = \pi/4$ is selected for comparison. Two different values of $\omega r/c_o$ are used: 0.2π (Fig. 2a) for $\omega r/c_o \sim 1$ and 100π (Fig. 2b) for $\omega r/c_o >> 1$. The solid lines are the MAE results, and the dashed lines are the CGF results. Figure 2(a) shows that when $\omega r/c_o$ is a small value, at which the CGF method does not apply, the MAE result is different both in magnitude and in phase from that of the CGF. When $\omega r/c_o$ becomes large in Fig. 2(b), the MAE and CGF solutions are the same. The fact that the results of Eqs. (7) and (22) are exactly the same also provides the evidence of the correctness in the procedure of reducing the MAE solution Eq. (7) to its acoustic far-field form Eq. (22). Figure 2 demonstrates graphically the consistency and differences between Eqs. (7) and (22).

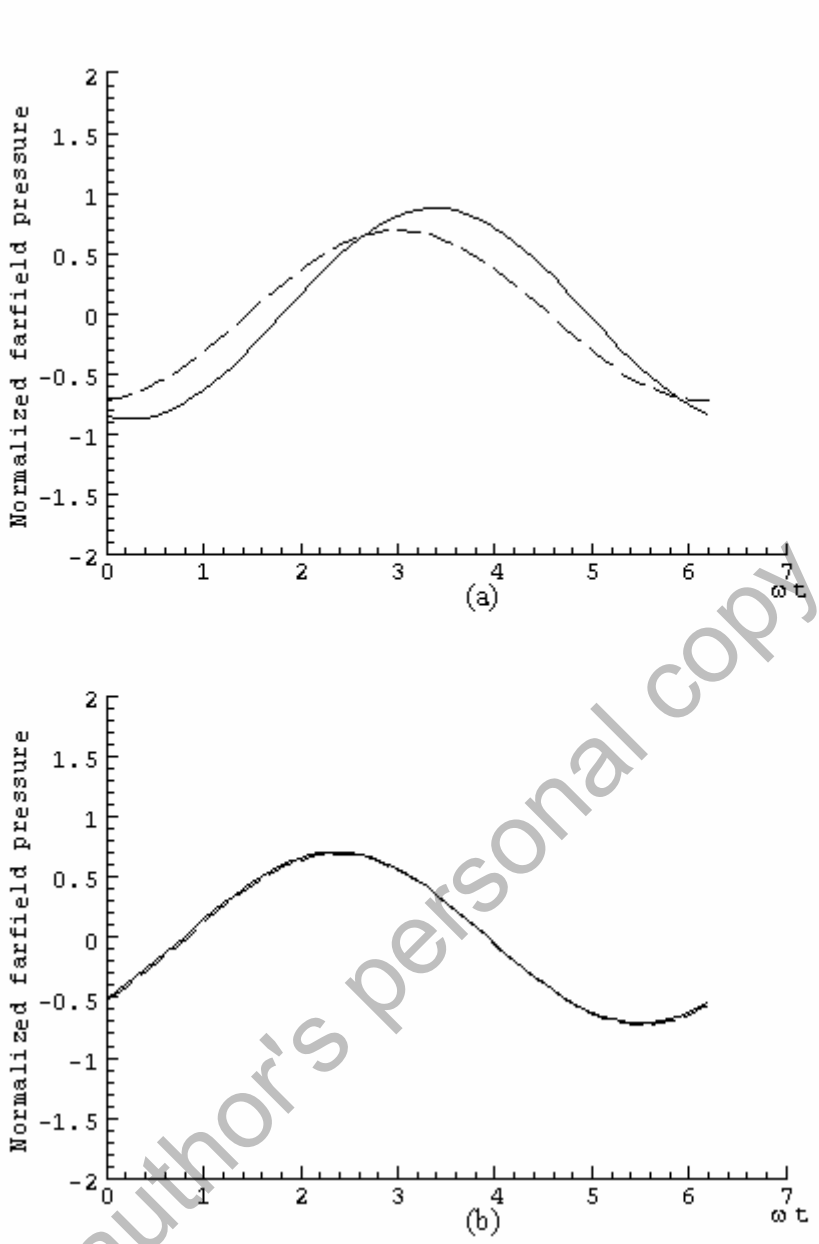

Figure 2. Far-field pressure (at the direction of $\theta=\pi/4$) comparisons using the MAE and CGF methods for the oscillating cylinder case. The solid lines represent the normalized MAE results from Eq. (7). The dashed lines represent the normalized CGF results from Eq. (22). (a) $\omega r / c_o = 0.2\pi$; (b) $\omega r / c_o = 100\pi$

4. VORTEX OUTSIDE A CYLINDER

The problem of a vortex outside a cylinder is shown in Fig. 3. Both the flow-field and the far field sound using the CGF method are presented in [5]. The sound is produced due to the unsteady motion of the vortex and its image at a^2 / z_o^*, where a is the radius of the cylinder, z_o is the position of the vortex in a complex variable format, and z_o^* is the complex conjugate of z_o. The image at the origin does not have any contribution to the sound because it does not have motion. Notice that all the three vortices have a constant circulation value. A

vortex with circulation of $\Gamma < 0$ is placed outside the cylinder so that the vortex trajectory is a circle traversing in the counter-clockwise direction with a constant radius r_o at speed

$$\upsilon_o = -\frac{\Gamma a^2}{2\pi r_o (r_o^2 - a^2)}, \tag{24}$$

and the angular speed of the rotation motion of the vortex is thus positive, equal to

$$\Omega = \frac{\upsilon_o}{r_o}. \tag{25}$$

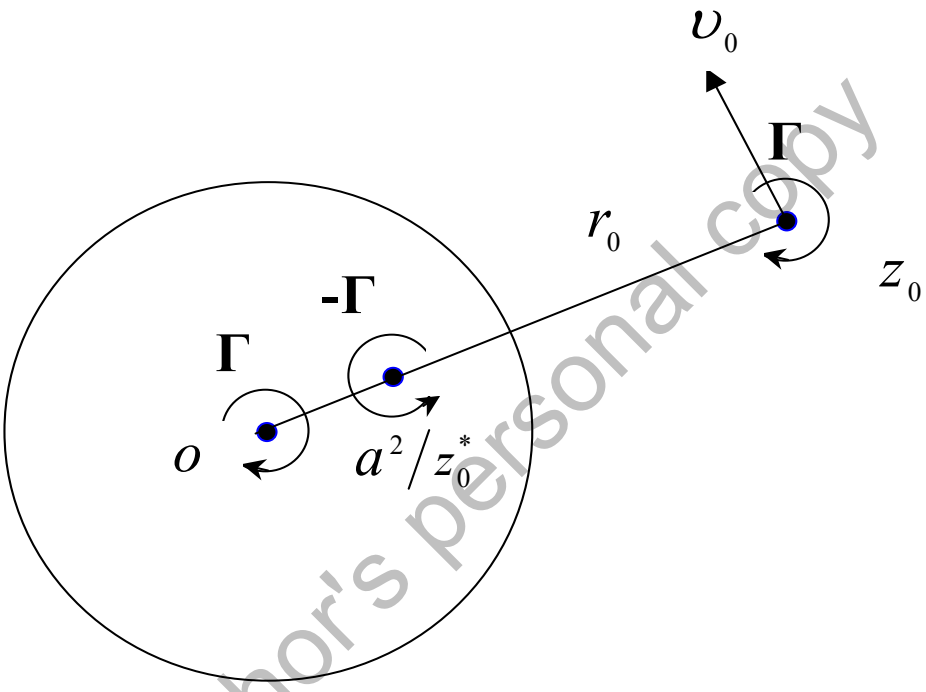

Figure 3. A vortex outside a circular cylinder

Using υ_o and a to non-dimensionalize the system and denoting vortex 1 as the vortex outside the cylinder and vortex 2 as the image inside the cylinder result in

$$\begin{aligned}(x_1, y_1) &= \frac{r_o}{a}(\cos\omega_o^*\tau, \sin\omega_o^*\tau),\\ (x_2, y_2) &= \frac{a}{r_o}(\cos\omega_o^*\tau, \sin\omega_o^*\tau),\end{aligned} \tag{26}$$

where ω_o^* and τ are dimensionless angular speed and time, respectively, and are expressed as

$$\begin{aligned}\omega_o^* &= \Omega\frac{a}{\upsilon_o} = \frac{a}{r_o},\\ \tau &= t\frac{\upsilon_o}{a}.\end{aligned} \tag{27}$$

The procedure of deriving the CGF solution is given in Ref. 5 and thus not repeated here. The derivation of the MAE solution is presented. Using Kao's MAE formula [6], the dimensionless acoustic pressure in the frequency domain can be expressed as

$$\hat{p}^* = -\frac{i\Gamma_j M_o \omega^*}{4\upsilon_o a} H_1^{(2)}(\omega^* R)\left[\sin\theta\int_{-\infty}^{\infty}\frac{Dx_j}{D\tau}e^{-i\omega^*\tau}d\tau - \cos\theta\int_{-\infty}^{\infty}\frac{Dy_j}{D\tau}e^{-i\omega^*\tau}d\tau\right], \tag{28}$$

where j=1, 2 and the Einstein summation convention is used, $\Gamma_1 = \Gamma$ and $\Gamma_2 = -\Gamma$, M_o is the Mach number defined as υ_o / c_o, and R is the dimensionless acoustic receiver distance defined as $M_o r / a$ with r the dimensional receiver distance. From Eq. (26), it can be deduced

$$\begin{aligned}\left(\frac{Dx_1}{D\tau}, \frac{Dy_1}{D\tau}\right) &= (-\sin\omega_o^*\tau, \cos\omega_o^*\tau),\\ \left(\frac{Dx_2}{D\tau}, \frac{Dy_2}{D\tau}\right) &= \frac{a^2}{r_o^{\,2}}(-\sin\omega_o^*\tau, \cos\omega_o^*\tau).\end{aligned} \tag{29}$$

Substituting the above expressions into Eq. (28), it can be obtained

$$\begin{aligned}\hat{p}^* &= -\frac{i\Gamma M_o \omega^*}{4\upsilon_o a} H_1^{(2)}(\omega^* R)\left(1-\frac{a^2}{r_o^2}\right)\\ &[\sin\theta\int_{-\infty}^{\infty}(-\sin\omega_o^*\tau)e^{-i\omega^*\tau}d\tau - \cos\theta\int_{-\infty}^{\infty}\cos\omega_o^*\tau e^{-i\omega^*\tau}d\tau].\end{aligned} \tag{30}$$

Using the δ-function, Eq. (30) can be written as

$$\begin{aligned}\hat{p}^* &= \frac{i\Gamma M_o \omega^* \pi}{4\upsilon_o a} H_1^{(2)}(\omega^* R)\left(1-\frac{a^2}{r_o^2}\right)\{i\sin\theta[\delta(\omega^*+\omega_o^*) - \delta(\omega^*-\omega_o^*)]\\ &+\cos\theta[\delta(\omega^*+\omega_o^*) + \delta(\omega^*-\omega_o^*)]\}.\end{aligned} \tag{31}$$

Taking an inverse Fourier transform of Eq. (31) to get

$$\begin{aligned}p^* &= \frac{i\Gamma M_o}{8\upsilon_o a}\left(1-\frac{a^2}{r_o^2}\right)\{i\sin\theta[-\omega_o^* H_1^{(2)}(-\omega_o^* R)e^{-i\omega_o^*\tau} - \omega_o^* H_1^{(2)}(\omega_o^* R)e^{i\omega_o^*\tau}]\\ &+\cos\theta[-\omega_o^* H_1^{(2)}(-\omega_o^* R)e^{-i\omega_o^*\tau} + \omega_o^* H_1^{(2)}(\omega_o^* R)e^{i\omega_o^*\tau}]\}.\end{aligned} \tag{32}$$

Defining

$$\begin{aligned}A &= H_1^{(2)}(\omega_o^* R) - H_1^{(2)}(-\omega_o^* R),\\ B &= H_1^{(2)}(\omega_o^* R) + H_1^{(2)}(-\omega_o^* R),\end{aligned} \tag{33}$$

Eq. (32) can be rewritten as

$$\begin{aligned}p^* &= \frac{i\Gamma M_o}{8\upsilon_o a}\left(1-\frac{a^2}{r_o^2}\right)\omega_o^*\{-i\sin\theta[B\cos\omega_o^*\tau + iA\sin\omega_o^*\tau] + \cos\theta[A\cos\omega_o^*\tau + iB\sin\omega_o^*\tau]\}\\ &= \frac{i\Gamma M_o}{8\upsilon_o a}\left(1-\frac{a^2}{r_o^2}\right)\omega_o^*\{A\cos(\theta-\omega_o^*\tau) - iB\sin(\theta-\omega_o^*\tau)\}.\end{aligned} \tag{34}$$

In Eq. (33), notice

$$H_1^{(2)}(x) = J_1(x) - iY_1(x), \tag{35}$$

where J_1 is the Bessel function of the first kind of order one, and Y_1 is the Bessel function of the second kind of order one. The definition of J_1 and Y_1 in [10] gives

$$\begin{aligned} J_1(-\omega_o^* R) &= -J_1(\omega_o^* R), \\ Y_1(-\omega_o^* R) &= -Y_1(\omega_o^* R) + 2i\,\mathrm{sgn}(\omega_o^* R) J_1(\omega_o^* R). \end{aligned} \tag{36}$$

When $R>0$ and $\omega_o^* > 0$, Eq. (33) gives

$$\begin{aligned} A &= -2iY_1(\omega_o^* R), \\ B &= 2J_1(\omega_o^* R). \end{aligned} \tag{37}$$

Substitution of Eq. (37) into Eq. (34) leads to

$$p^* = \frac{\Gamma M_o}{4\upsilon_o a}\left(1 - \frac{a^2}{r_o^2}\right)\omega_o^* \left\{Y_1(\omega_o^* R)\cos(\theta - \omega_o^* \tau) + J_1(\omega_o^* R)\sin(\theta - \omega_o^* \tau)\right\}. \tag{38}$$

This is the result by using the MAE method for the acoustic pressure fluctuation in the time domain.

To compare the CGF result at the acoustic far-field, further assume that $\omega_o^* R \to +\infty$. This condition leads to the asymptotic expressions as

$$\begin{aligned} Y_1(\omega_o^* R \to +\infty) &= \sqrt{\frac{2}{\pi\omega_o^* R}}\sin\left(\omega_o^* R - \frac{3\pi}{4}\right), \\ J_1(\omega_o^* R \to +\infty) &= \sqrt{\frac{2}{\pi\omega_o^* R}}\cos\left(\omega_o^* R - \frac{3\pi}{4}\right). \end{aligned} \tag{39}$$

Substitute Eq. (39) into Eq. (38) to get

$$p^* = \frac{\Gamma M_o}{2\upsilon_o a}\sqrt{\frac{\omega_o^*}{2\pi R}}\left(1 - \frac{a^2}{r_o^2}\right)\sin\left(\theta - \omega_o^* \tau + \omega_o^* R - \frac{3\pi}{4}\right). \tag{40}$$

To compare with the solution in a dimensional form given in [5], Eq. (40) can be dimensionalized to give

$$\begin{aligned} p(r,t) &= -\rho_o \upsilon_o^2 \sqrt{M_o}\sqrt{\frac{\pi r_o}{2r}}\left(\frac{r_o}{a}\right)^2\left(1 - \frac{a^2}{r_o^2}\right)^2 \sin\left\{\theta - \Omega\left[t - \frac{r}{c}\right] - \frac{3\pi}{4}\right\} \\ &= \rho_o \upsilon_o^2 \sqrt{M_o}\sqrt{\frac{\pi r_o}{2r}}\left(\frac{r_o}{a}\right)^2\left(1 - \frac{a^2}{r_o^2}\right)^2 \sin\left\{\theta - \Omega\left[t - \frac{r}{c}\right] + \frac{\pi}{4}\right\}. \end{aligned} \tag{41}$$

Again notice that the solution in [5] is for $\Omega < 0$ because a positive circulation vortex was placed outside the cylinder resulting in a clockwise rotation. For the positive (counter-clockwise) rotation, the formula on page 142 in [5] gives a phase angle of $+\pi/4$, instead of $-\pi/4$. Therefore the CGF result in [5] for the positive Ω case turns out to be the same as Eq. (41), which shows a typical two-dimensional dipole amplitude proportional to

$\rho_o v_o^2 \sqrt{M_o}$ and a cylindrically diverging acoustic wave decaying at $1/\sqrt{r}$ rate. The dipole lobes rotate counter-clockwise at an angular speed of Ω.

Figure 4 compares the results of the acoustic pressure variation with time using the MAE and CGF methods for this case of a vortex outside a cylinder, similar to Fig. 2 for the oscillating cylinder case. The results are calculated using the MAE method Eq. (38) and the CGF method Eq. (41). Equation (38) is applicable for any values of $\Omega r/c_o \sim O(1)$ as long as $M_o << 1$, while Eq. (41) is only valid when $\Omega r/c_o \to \infty$ (equivalent to $\omega^* R \to \infty$). The acoustic pressure in Fig. 4 is normalized with the coefficient in Eq. (41), $\rho_o v_o^2 \sqrt{M_o} \sqrt{\frac{\pi r_o}{2r}} \left(\frac{r_o}{a}\right)^2 \left(1 - \frac{a^2}{r_o^2}\right)^2$. The time variation is in the range of Ωt from 0 to 2π. A representative direction of the receiver location at $\theta=\pi/4$ is selected for comparison. Two different values of $\Omega r/c_o$ are used: 0.2π (Fig. 4a) for $\Omega r/c_o \sim 1$ and 100π (Fig. 4b) for $\Omega r/c_o >> 1$. Figure 4(a) shows that when $\Omega r/c_o$ is a small value, at which the CGF method does not apply, the MAE result is different both in magnitude and in phase from that of CGF. When $\Omega r/c_o$ becomes large in Fig. 4(b), the MAE and CGF solutions are the same. Again, when $\Omega r/c_o$ is large, the MAE result of Eq. (38) is identical to its acoustic far-field form of Eq. (41), demonstrating the correctness of the procedure when reducing the MAE solution Eq. (38) to its acoustic far-field form Eq. (41). Figure 4 demonstrates graphically the consistency and differences between Eqs. (38) and (41).

5. CONCLUSION

While both of the MAE method and the CGF method are limited to low Mach number flow, it is shown that the CGF method is more restrictive in terms of the far-field distance condition. The applicability of the MAE method is at the distance of $O(l/M)$, and the applicability of the CGF method is at a farther away location of $O(l/M^n)$ with $n>1$. This difference in the two methods can also be interpreted as the acoustic far-field requirement of $\omega r/c_o \to \infty$ for the CGF solutions and of $\omega r/c_o \sim 1$ for the MAE solutions. When $\omega r/c_o \sim 1$, the results from the two methods show significant differences in magnitude and phase. The MAE solution can be reduced to its acoustic far-field form and is shown to become identical to its corresponding CGF solution. Although there are other less restrictive formulae that can be used for flow generated acoustics (e.g., [11] and [12]), they are mostly used for numerical computation. The MAE and CGF methods can result in analytical far-field solutions.

There can be recommended values as for what constant should be chosen instead of the "order of magnitude" symbol for the far-field distance in practical computations for needed accuracy of the solution and what values of n should be selected for the same purpose. In practical computations, these values depend on the Mach number in the specific application. In an example of Mach number around 0.1, the far-field distance for a valid MAE solution

can be in the range of $0.5l/M$ and larger, and the far-field distance for a valid CGF is approximately in the range of l/M^2 and larger.

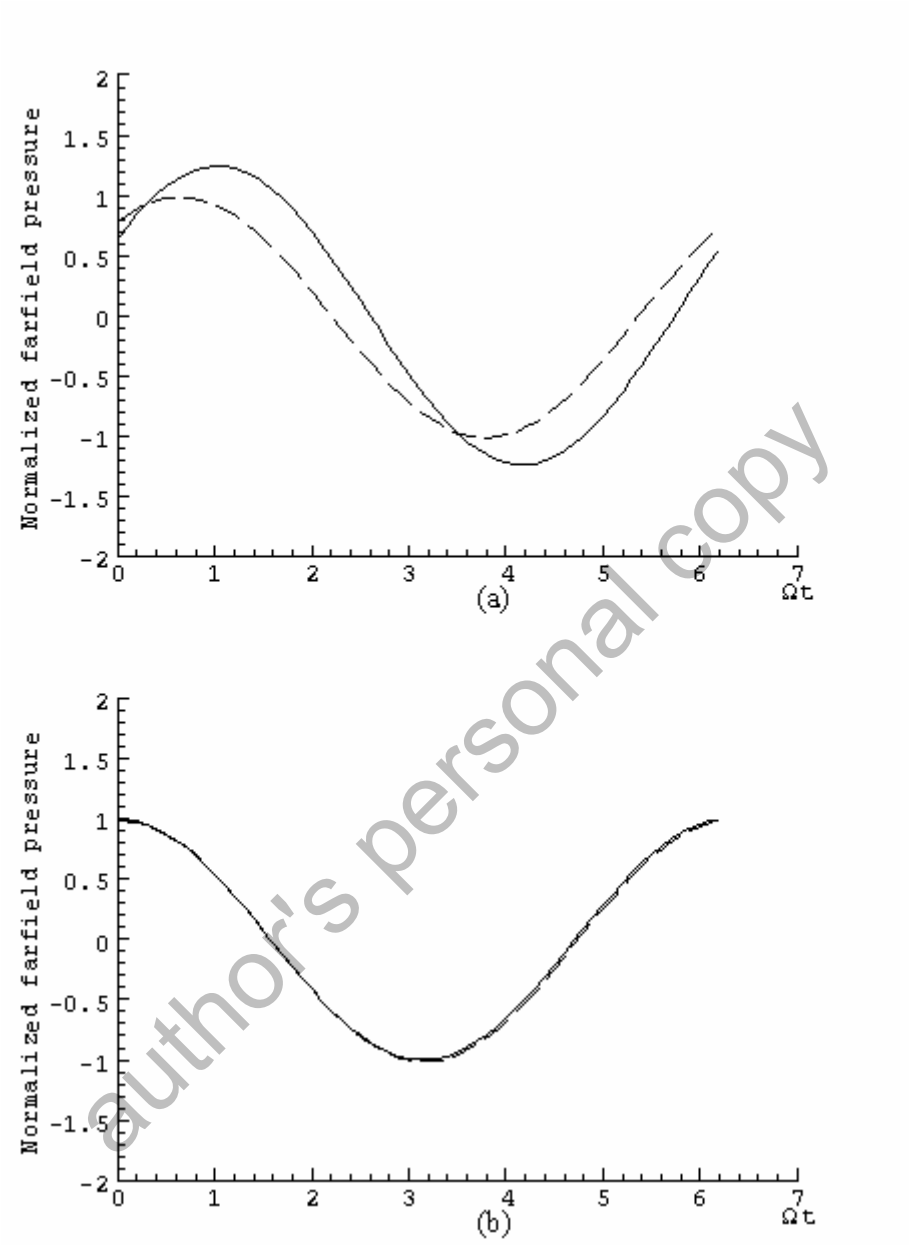

Figure 4. Far-field pressure (at the direction of $\theta=\pi/4$) comparisons using the MAE and CGF methods for the oscillating cylinder case. The solid lines represent the normalized MAE results from Eq. (38). The dashed lines represent the normalized CGF results from Eq. (41). (a) $\omega r/c_o = 0.2\pi$; (b) $\omega r/c_o = 100\pi$.

REFERENCES

1. Lighthill M. J. On sound generated aerodynamically I. General theory. Proceedings of the Royal Society of London, 1952, A 211, 564–587.
2. Lighthill M. J. On sound generated aerodynamically II. Turbulence as a source of sound. Proceedings of the Royal Society of London, 1954, A 222, 1–32.
3. Howe M. S. Trailing edge noise at low Mach numbers. Journal of Sound and Vibration, 1999, 225, 211–238.
4. Howe M. S. Edge-source acoustic Green's function for an airfoil of arbitrary chord with application to trailing-edge noise. The Quarterly Journal of Mechanics and Applied Mathematics, 2001, 54, 139–155.
5. Howe M. S. Theory of Vortex Sound. Cambridge University Press, Cambridge, U. K., 2003.
6. Kao H. C. Body-vortex interaction, sound generation, and destructive interference. AIAA Journal, 2002, 40, 652–660.
7. Crighton D. C. Radiation from vortex filament motion near a half plane. Journal of Fluid Mechanics, 1972, 51, 357–362.
8. Dowling A. P., Ffowcs Williams J. E. Sound and Sources of Sound. John Wiley and Sons, New York, 1983.
9. Abramowitz M., Stegun I. A. Handbook of Mathematical Functions. Dover, New York, 1965.
10. Kakac S., Yener Y. Heat Conduction. 3-rd edition, Taylor and Francis. Washington, DC, 1993.
11. Ffowcs Williams J. E., Hawkings D. L. Sound generation by turbulence and surface in arbitrary motion. Philosophical Transactions of the Royal Society of London, 1969, A 264, 321–342.
12. Wang M., Moin P. Computation of trailing-edge flow and noise using large-eddy simulation. AIAA Journal, 2000, 38, 2201–2209.